

Diffusion and percolation in anisotropic random barrier models

Sebastian Bustingorry

Centro Atómico Bariloche, 8400 San Carlos de Bariloche, Río Negro, Argentina

(Received 29 October 2003; published 24 March 2004)

An anisotropic random barrier model is presented, in which the transition probabilities in different directions have different probability density functions. At low temperatures, the anisotropic long-time diffusion coefficients, obtained using an effective medium approximation, follow an Arrhenius temperature dependence, with the same activation energy for each direction. Such activation energy is related to the anisotropic percolation properties of the lattice, and can be analyzed in terms of the critical percolation path approximation. The anisotropic effective medium approximation is shown to predict the correct percolation threshold for an anisotropic two-dimensional square lattice. In addition, results are compared with numerical simulations using a fast kinetic Monte Carlo algorithm.

DOI: 10.1103/PhysRevE.69.031107

PACS number(s): 05.40.-a, 05.60.Cd, 66.30.-h

I. INTRODUCTION

Diffusion in disordered media is an active field of research, due to its relevance in a wide variety of natural and industrial processes [1–3]. One of the traditional models for disorder is the random barrier model (RBM), which consists of equally energy minima separated by energy barriers, the height of which is randomly distributed according to a given probability density function (PDF). In this model, a particle moves from one minimum to another by performing thermally activated jumps.

In these systems, diffusion properties can be studied either in time or frequency variables. Several studies of diffusion properties have been conducted in the isotropic RBM both under unbiased [4–9] and biased [10,11] conditions. Following a frequency analysis (Refs. [4,5], and references therein), the system may be characterized by a zero-frequency diffusion constant $D(s=0)$, and a characteristic frequency s^* , which marks the onset of frequency-dependent diffusion. $D(s=0)$ and s^* follow Arrhenius laws with the same activation energy E_c . Analogously, from a time variable standpoint, it takes a time $t^* \sim s^{*-1}$ for a particle to reach a long-time diffusion regime in the RBM, characterized by a diffusion constant $D(t \rightarrow \infty) \equiv D(s=0)$ [8]. The activation energy E_c depends on the percolation properties of the lattice and the PDF of the energy barriers. This dependence is simply achieved by the critical percolation path approximation (CPPA), as shown for isotropic problems [12–14].

In view of the diversity of systems in which diffusion takes place, the anisotropic generalization of diffusion problems has attracted considerable attention in the last years, both under unbiased [15–21] and biased [22–24] conditions. A few examples of anisotropic systems are porous reservoir rocks [3,21,25], layered semiconducting compounds [26], and superconductor cuprates [27]. When dealing with anisotropic conditions, diffusion properties are independently studied in the different relevant directions of the system. It was recently shown that, for a two-dimensional anisotropic bond percolation model, different activation energies are found in each direction [20].

In the present paper, a two-dimensional unbiased diffusion process is studied with each direction characterized by a

different continuous PDF. The paper is organized as follows. In Sec. II the anisotropic RBM is introduced. In Sec. III, the model is studied within the anisotropic effective medium approximation (EMA). These results are compared against Monte Carlo simulations, whose numerical details are given in Sec. IV. Section V is devoted to a description of the CPPA ideas in anisotropic conditions, and in Sec. VI the concluding remarks of the present paper are presented.

II. ANISOTROPIC RANDOM BARRIER MODEL

Diffusion processes will be studied on a two-dimensional square lattice with static disorder. Energy barriers are chosen from a given PDF $\rho(E)$ at $t=0$ and are kept constant during the diffusion process. Possible jumps are only allowed between nearest neighbors. Once the energy barrier E_{ij} between sites i and j is selected, the transition rates ω_{ij} from site i to site j are determined following an Arrhenius law:

$$\omega_{ij} = \frac{\omega_0}{z} e^{-\beta E_{ij}}, \quad (1)$$

where ω_0 is the constant jump rate, $z=4$ is the coordination number, and $\beta=1/k_B T$ is the inverse temperature, with k_B being the Boltzmann constant. The energy E_{ij} characterizes the bond joining sites i and j , therefore $E_{ij}=E_{ji}$, and the forward ($i \rightarrow j$) and backward ($j \rightarrow i$) jumps have the same transition rate.

In order to introduce the anisotropic character of the system, the E_{ij} energies are selected from different PDFs, depending on the orientation of the bond joining sites i and j . Let 1 and 2 be the main directions of the square lattice, the key idea is to introduce $\rho_1(E_1)$ and $\rho_2(E_2)$ instead of a single PDF $\rho(E)$. The model is characterized by anisotropy $\alpha = \epsilon_1/\epsilon_2$ and global mean energy $\epsilon = (\epsilon_1 + \epsilon_2)/2$. The mean energies in each direction, ϵ_1 and ϵ_2 , are thus represented by $\epsilon_1 = 2\alpha\epsilon/(\alpha+1)$ and $\epsilon_2 = 2\epsilon/(\alpha+1)$. In the present work, a constant value of $\epsilon = 0.5\epsilon_0$ is adopted, where ϵ_0 sets the unit of energy, and the effects of having $\alpha \neq 1$ are studied. Two different anisotropic distributions will be considered: (a) an exponential PDF

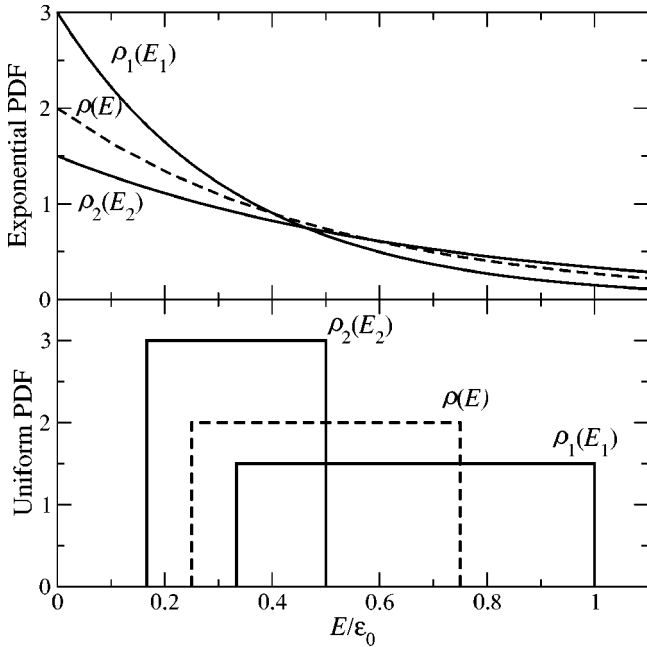


FIG. 1. Exponential (upper panel) and uniform (lower panel) probability density functions. Solid lines represent the anisotropic cases ($\alpha=2$) and dashed lines the isotropic cases.

$$\rho_1(E_1) = \frac{1}{\epsilon_1} e^{-E_1/\epsilon_1}, \quad E_1 \in [0, \infty),$$

$$\rho_2(E_2) = \frac{1}{\epsilon_2} e^{-E_2/\epsilon_2}, \quad E_2 \in [0, \infty), \quad (2)$$

and (b) a uniform PDF

$$\rho_1(E_1) = \frac{1}{2\delta_1\epsilon_1}, \quad E_1 \in [(1-\delta_1)\epsilon_1, (1+\delta_1)\epsilon_1],$$

$$\rho_2(E_2) = \frac{1}{2\delta_2\epsilon_2}, \quad E_2 \in [(1-\delta_2)\epsilon_2, (1+\delta_2)\epsilon_2], \quad (3)$$

where δ_1 and δ_2 serve to control different distribution widths in each direction. This uniform PDF represents the most general anisotropic extension of the isotropic uniform PDF used in Ref. [8] to study diffusion in RBM. In the following, and for the sake of simplicity, the widths of the uniform PDF will be $\delta_1 = \delta_2 = 0.5$. Figure 1 shows the exponential and uniform PDFs for $\alpha=1$ and $\alpha=2$.

III. ANISOTROPIC EMA: LOW TEMPERATURE PREDICTIONS

The EMA self-consistent conditions provide a method for obtaining the diffusion coefficients for a given disordered medium. Usually, these equations must be numerically solved, except for some simple cases. It is showed in this section that for the low temperature limit, some analytical predictions may be obtained within the RBM.

A. Self-consistent conditions

Many authors [28–31] have derived the EMA, which provides a self-consistent method to obtain effective diffusion coefficients. The approach considers one impure bond of the disordered lattice as embedded in an *effective medium*, mimicking the average surroundings. By imposing the averaged fluctuations to be zero, the self-consistent condition is derived for the transition rate of the effective medium. For an hypercubic d -dimensional isotropic lattice in the long-time limit, this condition reads [2]

$$\left\langle \frac{(\omega - \sigma)}{\omega + (d-1)\sigma} \right\rangle_{\nu(\omega)} = 0, \quad (4)$$

where ω is the transition rate of the impure bond distributed according to the PDF $\nu(\omega)$, σ is the transition rate of the effective medium, and the brackets denote average over the PDF $\nu(\omega)$. Solving the self-consistent condition for σ , the diffusion coefficient is obtained as $D = \sigma a^2$, where a is the lattice constant.

The anisotropic extension of such formalism, where there exist n different directions, leads to n coupled equations that self-consistently solve for the n different diffusion coefficients. In a two-dimensional square lattice, and for the long-time limit, these conditions are [16,18]

$$\left\langle \frac{(\omega_m - \sigma_m)}{\omega_m + (f_{mn}^{-1} - 1)\sigma_m} \right\rangle_{\nu_m(\omega_m)} = 0, \quad (5)$$

with

$$f_{mn} = \frac{2}{\pi} \arctan \sqrt{\frac{\sigma_m}{\sigma_n}} \quad (6)$$

and $m, n = 1, 2$ denoting the principal axes of the lattice. The effective transition rates σ_i are related to the diffusion constants by $D_i = \sigma_i a^2$.

At high temperatures, the particle can easily overcome energy barriers, and eventually all diffusion constants approach the same value. In Fig. 2, the normalized diffusion coefficients at high temperatures for the two-dimensional square lattice with an exponential PDF are plotted as functions of temperature, both under isotropic and anisotropic conditions. Lines represent the solutions of the EMA self-consistent conditions, Eqs. (4) and (5), and symbols correspond to numerical simulations (see Sec. IV). The figure shows that, for high temperatures, $D_i/a^2\omega_0 \rightarrow 1/z$. Analogous results are obtained using the uniform PDF. In the following sections the predictions of EMA for diffusion at low temperatures are considered.

B. Isotropic case

For an isotropic hypercubic lattice in d dimensions, Eq. (4) may be written as

$$\left\langle \frac{(\omega + (d-1)\sigma - d\sigma)}{\omega + (d-1)\sigma} \right\rangle_{\nu(\omega)} = 0. \quad (7)$$

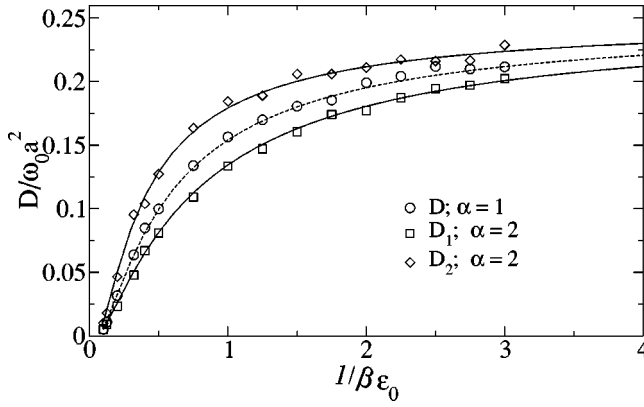


FIG. 2. Diffusion coefficients at high temperatures. Lines correspond to the EMA solution and symbols to numerical simulations. The isotropic case is represented by a dashed line and the anisotropic case $\alpha=2$ by continuous lines.

By introducing the explicit dependence on energy $\omega = \omega(E)$ given in Eq. (1), and transforming the transition rate average over $\nu(\omega)$ to an energy average over $\rho(E)$, Eq. (7) becomes

$$\left\langle \frac{1}{\omega(E) + (d-1)\sigma} \right\rangle_{\rho(E)} = \frac{1}{d\sigma}. \quad (8)$$

For $\beta \rightarrow \infty$ the transition rate $\omega(E)$ varies extremely rapidly, due to its exponential dependence. Therefore it is possible to define an energy value E_c such that two possibilities arise: $\omega(E) \gg (d-1)\sigma$ for $E < E_c$ or $\omega(E) \ll (d-1)\sigma$ for $E > E_c$. The characteristic value E_c can be therefore defined as

$$\omega(E_c) = (d-1)\sigma. \quad (9)$$

For values of $E < E_c$, the left-hand side of Eq. (8) vanishes. Alternatively, for $E > E_c$ the value $\omega(E)$ on the left-hand side of Eq. (8) may be ignored. Taking these conditions into account, and averaging over $\rho(E)$, Eq. (8) for $\beta \rightarrow \infty$ becomes

$$\frac{1}{d\sigma} = \int_{E_c}^{\infty} \frac{\rho(E)}{(d-1)\sigma} dE, \quad (10)$$

or, equivalently,

$$\int_0^{E_c} \rho(E) dE = \frac{1}{d}. \quad (11)$$

In the EMA, the bond percolation threshold of the hypercubic lattice is given by $p_c^{EMA} = d^{-1}$ [28–31]. Therefore, Eq. (11) is a condition over E_c for each particular PDF $\rho(E)$, in terms of the percolation properties of the lattice. Indeed, combining this value of E_c with Eq. (9), the EMA diffusion coefficient for isotropic d -dimensional hypercubic lattices at low temperatures is given by

$$D = \frac{\omega_0 a^2}{z(d-1)} e^{-\beta E_c}. \quad (12)$$

It is worth noting that $p_c^{EMA} = d^{-1}$ is only exact for $d=2$ [32], therefore Eq. (12) does not give the correct exponential behavior for $d=3$, and other approximations, such as CPPA, should be considered [7].

C. Anisotropic two-dimensional case

For the anisotropic two-dimensional case, Eq. (5) turns into two self-consistent conditions, with transition rate PDFs $\nu_1(\omega_1)$ and $\nu_2(\omega_2)$, for each direction of the lattice. By introducing the energy dependence $\omega_1 = \omega(E_1)$ and $\omega_2 = \omega(E_2)$, the two self-consistent conditions read

$$\left\langle \frac{1}{\omega(E_1) + (f_{12}^{-1} - 1)\sigma_1} \right\rangle_{\rho_1(E_1)} = \frac{f_{12}}{\sigma_1},$$

$$\left\langle \frac{1}{\omega(E_2) + (f_{21}^{-1} - 1)\sigma_2} \right\rangle_{\rho_2(E_2)} = \frac{f_{21}}{\sigma_2}. \quad (13)$$

Again, the PDFs change abruptly for $\beta \rightarrow \infty$, and a parameter E_c can be defined as in the isotropic case. However, E_c is expected to be characteristic of the underlying energy landscape, so the diffusion coefficients in each direction are expected to be governed by a single E_c . For the anisotropic case, an energy E_c will be defined separating two limiting conditions simultaneously: $\omega(E_1) \ll (f_{12}^{-1} - 1)\sigma_1$ and $\omega(E_2) \ll (f_{21}^{-1} - 1)\sigma_2$ for E_1 and E_2 larger than E_c , and $\omega(E_1) \gg (f_{12}^{-1} - 1)\sigma_1$ and $\omega(E_2) \gg (f_{21}^{-1} - 1)\sigma_2$ for E_1 and E_2 smaller than E_c . Thus, E_c must verify two simultaneous conditions

$$\omega(E_c) = (f_{12}^{-1} - 1)\sigma_1,$$

$$\omega(E_c) = (f_{21}^{-1} - 1)\sigma_2. \quad (14)$$

In this way, a set of equations analogous to Eq. (11) are obtained,

$$\int_0^{E_c} \rho_1(E_1) dE_1 = f_{12},$$

$$\int_0^{E_c} \rho_2(E_2) dE_2 = f_{21}. \quad (15)$$

By adding Eqs. (15), using Eq. (6) and trigonometric relations, an expression is arrived at,

$$\int_0^{E_c} \rho_1(E_1) dE_1 + \int_0^{E_c} \rho_2(E_2) dE_2 = 1, \quad (16)$$

which gives the activation energy E_c as a function of the anisotropy α . Moreover, by replacing the expressions in Eqs. (15) for f_{12} and f_{21} in Eqs. (14), and solving for σ_1 and σ_2 , the corresponding anisotropic diffusion coefficients are obtained:

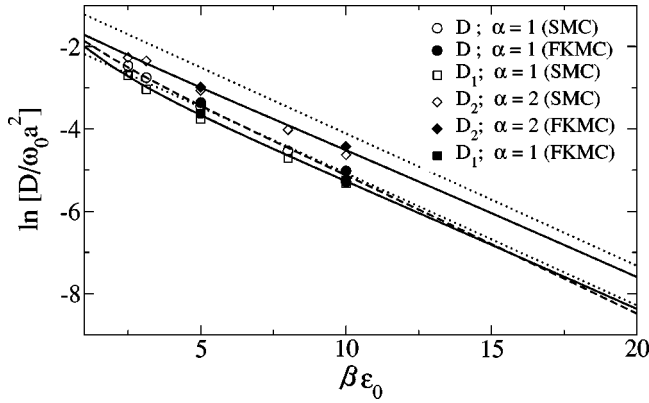


FIG. 3. Arrhenius plot of the diffusion coefficients for an exponential PDF. The solution of the self-consistent EMA conditions is represented with a dashed line for the isotropic case and with continuous lines for the anisotropic $\alpha=2$ cases. Dotted lines represent the analytical EMA predictions, Eqs. (17), for low temperatures. Symbols correspond to SMC (standard Monte Carlo) and FKMC (fast kinetic Monte Carlo) simulations, as indicated.

$$D_1 = \frac{\int_0^{E_c} \rho_1(E_1) dE_1}{\int_0^{E_c} \rho_2(E_2) dE_2} \frac{\omega_0 a^2}{z} e^{-\beta E_c},$$

$$D_2 = \frac{\int_0^{E_c} \rho_2(E_2) dE_2}{\int_0^{E_c} \rho_1(E_1) dE_1} \frac{\omega_0 a^2}{z} e^{-\beta E_c}. \quad (17)$$

The isotropic result, Eq. (12), is obviously recovered by setting $\rho_1 = \rho_2$.

Figures 3 and 4 show Arrhenius plots of the anisotropic diffusion coefficients at low temperatures, corresponding to the exponential and uniform PDFs, respectively. The solution

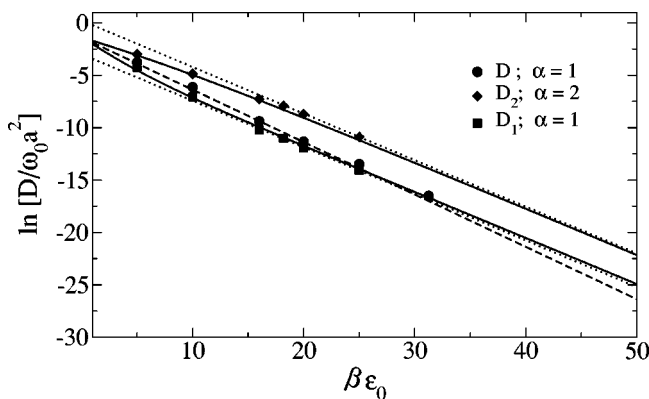


FIG. 4. Arrhenius plot of the diffusion coefficients for a uniform PDF. The solution of the self-consistent EMA conditions is represented with a dashed line for the isotropic case and with continuous lines for the anisotropic $\alpha=2$ cases. Dotted lines represent the analytical EMA predictions, Eqs. (17), for low temperatures. Symbols correspond to FKMC simulations.

of EMA self-consistent conditions, Eqs. (4) and (5), are represented with dashed and continuous lines, for the isotropic and anisotropic $\alpha=2$ cases, respectively. Dotted lines represent the prediction of EMA for the low temperature limit, Eqs. (17). Symbols are the results of numerical simulations, as described in the following section. These figures show that the diffusion coefficients in each direction follow Arrhenius laws with the same activation energy. Even though simulation data at lower temperatures are needed, the agreement with the low temperature anisotropic diffusion coefficients is better for a uniform PDF than for an exponential PDF.

IV. NUMERICAL SIMULATIONS

Monte Carlo simulations were performed to obtain long-time diffusion coefficients for comparison with anisotropic EMA predictions. The energy landscape was selected from the corresponding PDF at $t=0$ and kept fixed during the diffusion process. At $t=0$ a particle was assigned to a random initial site i . Different Monte Carlo algorithms may be used at this point and two possibilities were considered: standard Monte Carlo (SMC) [8] and a fast kinetic Monte Carlo (FKMC) [33] scheme. A brief description of these methods is given in the following.

In SMC, the particle selects at random one of its nearest neighbors j and tries to overcome the barrier between them in a time unit. A random number $\xi \in (0,1)$ is generated such that if $\xi < \omega_{ij}$ the jump is effective, otherwise the particle stays at the initial site. In this process, one unit of time is used for every jump trial. Although SMC simulations proved to be very useful for studying diffusion processes, it was shown that it is not too appropriate for studying low temperature regimes [5,8,33]. At low temperatures, the transition rates decrease exponentially with increasing β , and the random number ξ is, mostly, orders of magnitude greater than the transition rates, making the number of effective jumps (displacements) very small and the long-time diffusion regime difficult to reach.

In the FKMC [33] scheme, consider the particle in a site i on a lattice with its z nearest neighbors j ($j=1, \dots, z$). The transition rates from i to j are denoted by ω_{ij} . The total transition rate ω_i from site i is defined as

$$\omega_i = \sum_{j=1}^z \omega_{ji}. \quad (18)$$

Instead of selecting the neighbor at random, as in SMC, a neighbor k is selected for an effective jump given that

$$\frac{1}{\omega_i} \sum_{j=1}^{k-1} \omega_{ji} < \xi_1 \leq \frac{1}{\omega_i} \sum_{j=k}^z \omega_{ji}, \quad (19)$$

where ξ_1 is randomly uniformly distributed in $(0,1)$. The time variable t is then increased in t' , where t' is chosen from an exponential distribution with mean waiting time ω_i^{-1} . Therefore,

$$t' = -\frac{1}{\omega_i} \ln \xi_2, \quad (20)$$

with ξ_2 randomly uniformly distributed in $(0,1)$. This procedure is repeated from site k and so on. In the FKMC algorithm, each jump trial is effective, meaning that the particle always jumps to one of its neighbors, and the time elapsed in one jump is accordingly adjusted. Furthermore, the FKMC algorithm depends on the ratios ω_{ji}/ω_i and consequently it is not as β dependent as ω_{ji} [33]. This algorithm allows us to reach larger values of β in simulations of the diffusion process.

Simulations were performed on 300×300 and 500×500 sites square lattices for the SMC and FKMC, respectively, with periodic boundary conditions. For each algorithm, the mean square displacements on each direction $\langle r_1^2(t) \rangle$ and $\langle r_2^2(t) \rangle$ were computed, averaging over between 2000 and 5000 realizations of the random walks. The long-time diffusion coefficients were defined through $\langle r_{1(2)}^2(t) \rangle = 2D_{1(2)}t$, and were obtained from the best linear fits to the long-time mean square displacements.

In Figs. 3 and 4, numerical simulations and EMA results are presented together. In Fig. 3, SMC simulations are plotted up to $\beta\epsilon_0=10$ and some FKMC simulation points are shown for comparison. Both algorithms coincide within the numerical precision. In Fig. 4, only FKMC results are presented up to a value $\beta\epsilon_0=30$. Monte Carlo simulations do not completely reach the asymptotic low temperatures behavior. However, numerical simulations and EMA seem to agree very well in the accessible temperature range.

V. CRITICAL PERCOLATION PATH APPROXIMATION

The idea of a percolation path governing diffusion at low temperatures was first developed in Ref. [12] and rigorously proved later [13,14]. In this section, this idea will be briefly summarized and extended to anisotropic conditions.

At low temperatures the characteristic Arrhenius diffusion energy E_c can be related to the bond percolation threshold of the lattice. Consider a random walk on a realization of the disorder energy landscape at a very low temperature. In order to overcome a barrier with an energy E' , the particle spends a mean waiting time $t' \sim \exp(\beta E')$. For short times, therefore, the particle can only move to sites which are connected by low energy barriers and is surrounded by a perimeter of higher energy. Roughly, at time t' the particle might jump barriers with $E \leq E'$, and the probability to overcome this barriers is $\int_0^{E'} \rho(E) dE$. For longer times, the particle could overcome the lowest barrier of the perimeter, and access a new region with a higher energy perimeter. These regions are noncompact in the sense that they may have inside barriers that belong to the perimeter barriers. Eventually, there exists a particular barrier of height E_c , beyond which the particle gains access to the whole system, through the corresponding percolation path of energies $E \leq E_c$. Thus, for an isotropic medium, E_c is given by

$$\int_0^{E_c} \rho(E) dE = p_c, \quad (21)$$

where p_c is the bond percolation threshold of the system ($p_c=0.5$ for the two-dimensional isotropic square lattice

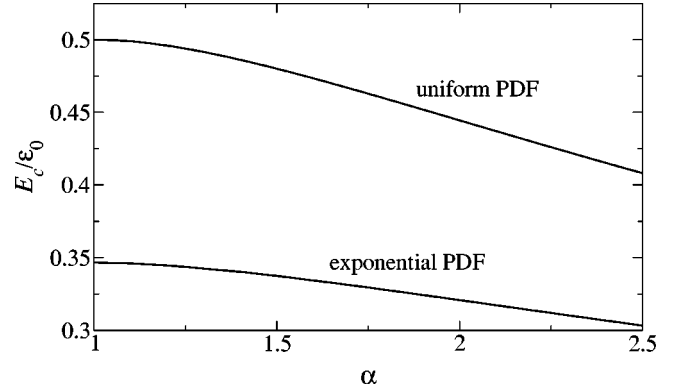


FIG. 5. Dependence of the activation energy E_c on the anisotropic parameter α for the exponential and uniform PDFs studied here.

[32]). It has been shown that E_c is the highest energy barrier which the particle must overcome in order to gain full access to the percolation network. The long-time diffusion coefficient must therefore be $D \sim \exp(-\beta E_c)$, which is indeed the observed behavior of isotropic diffusion at low temperatures [4,8].

The percolation threshold of a particular lattice, which is given by a point p_c for isotropic percolation, becomes for anisotropic percolation a critical surface $\varphi(\{p_i\})=0$ [34], where $\{p_i\}$ denotes the set of relevant occupation probabilities. For example, the percolation function is $\varphi(p)=p-p_c$ for isotropic percolation, $\varphi(p_1,p_2)=p_1+p_2-1$ for the square lattice, and $\varphi(p_1,p_2,p_3)=p_1+p_2+p_3-p_1p_2p_3-1$ for the triangular lattice [34]. Furthermore, the critical surface implies a change in the morphology of the incipient percolation network.

In the anisotropic RBM context, the occupation probabilities of a bond with energy barrier E , i.e., accessibility condition of the bond, is given by the probability of E being lower than the maximum accessible barrier. Therefore, the generalization of Eq. (21) to anisotropic conditions becomes

$$\varphi\left(\left\{\int_0^{E_c} \rho_i(E_i) dE_i\right\}\right) = 0. \quad (22)$$

Note that there exists just one energy E_c , which is the same for all directions, and gives full access to the whole anisotropic percolation network. For the anisotropic RBM on a square lattice, Eq. (22) becomes equal to the EMA prediction, Eq. (16). This means that EMA predicts the correct critical percolation surface $\varphi(p_1,p_2)=p_1+p_2-1$ for anisotropic bond percolation in the square lattice [15,17].

Figure 5 shows the effect of anisotropy α on $E_c(\alpha)$ for the energy distributions studied in the present model, and predicted both by CPPA, Eq. (22), and EMA, Eq. (16). For the exponential PDF, the condition for E_c reads $\exp(-E_c/\epsilon_1) + \exp(-E_c/\epsilon_2) = 1$, which was numerically solved. For the uniform PDF Eq. (16) gives $E_c/\epsilon_0 = 2\alpha/(\alpha+1)^2$.

VI. CONCLUDING REMARKS

In this paper, diffusion properties were studied using an anisotropic RBM, with emphasis on the low temperature be-

havior and on percolation properties. Two kind of PDFs were used to characterize different directions of the lattice, namely, exponential and uniform PDFs. The anisotropic EMA was used to calculate the long-time diffusion properties for all temperatures, derived from the numerical solutions of the self-consistent conditions expressed in Eqs. (5). Furthermore, analytical expressions for the diffusion coefficients at low temperatures were obtained, Eq. (17), which show that diffusion in different directions follows Arrhenius laws with a same activation energy E_c . This should be compared with the thermally activated diffusion in anisotropic bond percolation lattices, in which different activation energies are found for each direction [20]. In the present model, only one activation energy is found due to the existence of an anisotropic percolation path of low energy barriers, which governs the diffusion process. Besides giving the activation energy for diffusion, EMA predicts the exponential prefactor for diffusion and its dependence with the anisotropy of the disordered system.

The two Monte Carlo algorithms used here, namely, SMC and FKMC, show a very good agreement with the EMA predictions for the diffusion coefficients in the accessible temperature range. For a more extensive comparison with EMA, other algorithms should be used.

In the present paper, a connection was established between EMA and CPPA ideas, and EMA was shown to predict the correct activation energy for anisotropic diffusion in the square lattice. For other geometries and dimensions, it is expected that EMA will still predict an Arrhenius behavior, but with an activation energy that differs from that predicted by CPPA. This difference is due to the fact that CPPA uses the percolation threshold as a parameter, while EMA predicts its own percolation threshold. However, EMA is known to predict the correct percolation threshold only for the square lattice, even in anisotropic conditions [15,17]. Concerning CPPA, corrections of the form β^y become relevant for dimensions greater than two, but it is not clear which of both approximations, EMA or CPPA, give better results [7] and a systematic comparison turns necessary. Additional work in this direction is now under progress.

ACKNOWLEDGMENTS

The author want to thanks G. L. Insua for useful discussions. This work was financially supported by CONICET, Argentina.

-
- [1] J.W. Haus and K.W. Kehr, *Phys. Rep.* **150**, 263 (1987).
 - [2] J.P. Bouchaud and A. Georges, *Phys. Rep.* **195**, 127 (1990).
 - [3] M. Sahimi, *Flow and Transport in Porous Media and Fractured Rock* (VCH, Weinheim, Germany, 1995).
 - [4] J.C. Dyre, *Phys. Rev. B* **49**, 11 709 (1994).
 - [5] J.C. Dyre and T.B. Schroder, *Rev. Mod. Phys.* **72**, 873 (2000).
 - [6] I. Avramov, A. Milchev, and P. Argyrakis, *Phys. Rev. E* **47**, 2303 (1993).
 - [7] H. Ambaye and K.W. Kehr, *Phys. Rev. E* **51**, 5101 (1995).
 - [8] P. Argyrakis, A. Milchev, V. Pereyra, and K.W. Kehr, *Phys. Rev. E* **52**, 3623 (1995).
 - [9] A. Hörner, A. Milchev, and P. Argyrakis, *Phys. Rev. E* **52**, 3570 (1995).
 - [10] E. Arapaki, P. Argyrakis, I. Avramov, and A. Milchev, *Phys. Rev. E* **56**, R29 (1997).
 - [11] I. Avramov, A. Milchev, E. Arapaki, and P. Argyrakis, *Phys. Rev. E* **58**, 2788 (1998).
 - [12] V. Ambegaokar, B.I. Halperin, and J.S. Langer, *Phys. Rev. B* **4**, 2612 (1971).
 - [13] S. Tyc and B.I. Halperin, *Phys. Rev. B* **39**, 877 (1989).
 - [14] P.L. Doussal, *Phys. Rev. B* **39**, 881 (1989).
 - [15] J. Bernasconi, *Phys. Rev. B* **9**, 4575 (1974).
 - [16] P.E. Parris, *Phys. Rev. B* **36**, 5437 (1987).
 - [17] P.G. Toledo, H.T. Davis, and L.E. Scriven, *Chem. Eng. Sci.* **47**, 391 (1992).
 - [18] E.R. Reyes, M.O. Cáceres, and P.A. Pury, *Phys. Rev. B* **61**, 308 (2000).
 - [19] M.O. Cáceres and E.R. Reyes, *Physica A* **227**, 277 (1996).
 - [20] S. Bustingorry and G.L. Insua, *Phys. Rev. E* **68**, 012101 (2003).
 - [21] M. Saadatfar and M. Sahimi, *Phys. Rev. E* **65**, 036116 (2002).
 - [22] S. Bustingorry, E.R. Reyes, and M.O. Cáceres, *Phys. Rev. E* **62**, 7664 (2000).
 - [23] S. Bustingorry, M.O. Cáceres, and E.R. Reyes, *Phys. Rev. B* **65**, 165205 (2002).
 - [24] S.-Y. Huang, X.-W. Zou, and Z.-Z. Jin, *Phys. Rev. E* **65**, 052105 (2002).
 - [25] J.M.V.A. Koelman and A. de Kuijper, *Physica A* **247**, 10 (1997).
 - [26] L.K. Gallos, A.N. Anagnostopoulos, and P. Argyrakis, *Phys. Rev. B* **50**, 14 643 (1994).
 - [27] H. Jhans, D. Kim, R.J. Rasmussen, and J.M. Honig, *Phys. Rev. B* **54**, 11 224 (1996).
 - [28] S. Alexander, J. Bernasconi, W.R. Schneider, and R. Orbach, *Rev. Mod. Phys.* **53**, 175 (1981).
 - [29] T. Odagaki and M. Lax, *Phys. Rev. B* **24**, 5284 (1981).
 - [30] I. Webman, *Phys. Rev. Lett.* **47**, 1496 (1981).
 - [31] S. Summerfield, *Solid State Commun.* **39**, 401 (1981).
 - [32] D. Stauffer and A. Aharony, *Introduction to Percolation Theory* (Taylor & Francis, London, 1994).
 - [33] F.M. Bulnes, V.D. Pereyra, and J.L. Riccardo, *Phys. Rev. E* **58**, 86 (1998).
 - [34] G. Grimmet, *Percolation* (Springer-Verlag, Berlin, 1990).